На основі аналізу елементного складу матеріалів мішені з високоентропійного шестиелементного сплаву AlTiVCrNbMo і електронно-променевих покриттів на його основі встановлено критичний параметр (питома теплота випаровування елемента), який визначає селективну зміну елементного складу. Показано, що формування однофазного покриття високоентропійного сплаву відбувається, коли до складу покриття входить не менше 5 елементів. Отримані результати дозволяють обґрунтувати принципи підбору компонент для досягнення оптимальних елементного та фазового складу високоентропійних сплавів

Ключові слова: високоентропійний сплав AlTiVCrNbMo, електронно-променеве покриття, термічний фактор, елементний склад, фазовий склад

На основе анализа элементного состава материалов мишени из высокоэнтропийного шестиэлементного сплава AlTiVCrNbMo и электронно-лучевых покрытий на его основе установлен критичный параметр (удельная теплота испарения элемента), определяющий селективное изменение элементного состава. Показано, что формирование однофазного покрытия высокоэнтропийного сплава происходит, когда в состав покрытия входит не менее 5 элементов. Полученные результаты позволяют обосновать принципы подбора компонент для достижения оптимальных элементного и фазового состава высокоэнтропийных сплавов

Ключевые слова: высокоэнтропийный сплав AlTiVCrNbMo электронно-лучевое покрытие, термический фактор, элементный состав, фазовый состав

UDC 539.216.2: 544.02
DOI: 10.15587/1729-4061.2018.126545

INFLUENCE OF THE THERMAL FACTOR ON THE COMPOSITION OF ELECTRON-BEAM HIGH-ENTROPY ALTiVCrNbMo COATINGS

O. Sobol'
Doctor of Physics and Mathematics Sciences, Professor*
E-mail: sool@kpi.kharkov.ua
A. Barmin
PhD, Associate Professor*
S. Hryhorieva
Engineer*
V. Gorban'
Doctor of Technical Sciences
Frantsevich Institute for Problems of Materials Science
Krzhyzhanovskoho str., 3, Kyiv, Ukraine, 03680
A. Vuets
Junior Researcher*
A. Subbotin
Researcher*
*Department of Materials Science
National Technical University "Kharkiv Polytechnic Institute"
Kyrpychova str., 2, Kharkiv, Ukraine, 61002

1. Introduction

Structural engineering has recently become a basic method for achieving the required functional properties of materials [1, 2]. Owing to structural engineering, it became possible to create new types of materials. Such materials include pseudo-alloys [3], nanoperiodic composites based on various transient metals [4, 5], solid solutions, oversaturated as a result of ion implantation, based on metals [6] or phases of implantation [7]. It becomes possible to stabilize metastable structural states by selecting conditions for the formation of materials [8].

A separate direction of structural engineering is the creation of artificial materials based on multi-element composites [9], as well as multi-layer structures with alternating metal and ceramic layers [10]. Such artificial materials have unique high performance characteristics [11]. A particularly high increase in the functional characteristics was detected for the materials, which were formed under very non-equilibrium conditions [12, 13]. This is caused by ion bombardment at condensation that occurs at deposition of coatings in vacuum [14]. In this case, the higher selectivity for element composition can be achieved [15].

In recent years, special attention has been paid to coatings based on multi-element (high-entropy) alloys [16]. This is predetermined by that the high-entropy alloys have the unique property of ordering in a metal lattice at high temperatures [17]. Ordering is caused by the fact that the contribution of an entropy factor increases in high-entropy alloys as a result of intensive agitation [18], which stabilizes the formation of a solid solution with a simple crystalline structure [19] or amorphous-like state [20]. This makes it possible to attain high-temperature resistance to oxidation while retaining high physical-mechanical properties. Such properties of materials are extremely relevant and are required for parts and elements in modern aerospace technology, as well as power machine-building technologies.

2. Literature review and problem statement

To increase thermal stability of a material, the concept of multi-component high-entropy alloys (HEA) was proposed

and experimentally proved [21, 22]. In accordance with this concept, high entropy of mixing can stabilize the formation of a disordered solid-solution phase and prevent the formation of intermetallic phases in the process of crystallization [23].

The main feature of high-entropy alloys is the existence of heterogeneous atoms of elements in a lattice of the solid solution [24]. Atoms of multi-element high-entropy alloys have a different electron structure, dimensions, and thermodynamic properties in the crystal lattice of the solid solution of substitution. At an unordered arrangement, there occurs a significant distortion of the crystalline lattice. Emerging microdistortions of the crystalline lattice contribute to the solid solution hardening [25]. A decreased free energy of high-entropy alloys ensures stability of solid solution alloys at high temperatures [26]. In addition, large distortions of the lattice, due to the substitution of several metal elements with different atomic dimensions, lead to a decrease in the rate of atoms diffusion and intensify the effect of formation and stabilization of the solid solution [27]. Large distortions also contribute to a decrease in the rate of crystallites growth [28]. In this case, a nano-dimensional or amorphous structure is formed [29]. As a result of high entropy of mixing such alloys, lattice deformation and a decrease in the diffusion, the formation of solid solution phase with a simple crystalline lattice occurs in high-entropy alloys [30]. These crystal lattices are the face-centered cubic (FCC) or body-centered (BCC) lattices [31], but no double or triple intermetallic compounds are not formed in this case [32]. The importance of a difference in atomic radii of the constituent components was determined for the formed structural state [33]. In this case, the more constituent elements with very different atomic radii there are, the higher the probability for the formation of an amorphous-like state [34]. In this regard, all most commonly employed atoms of transient metals can be conditionally divided into several groups. The first group includes Si with a relatively small atomic radius (0.117 nm). The second group includes elements whose atomic radius is about 0.125 nm (Cr – 0.125 nm, Co – 0.125 nm, V – 0.132 nm, Fe – 0.126 nm, Cu – 0.128 nm, Ni – 0.124 nm). The third group includes elements whose atomic radius is about 0.145 nm (Al – 0.143 nm, Ta – 0.143 nm, Ti – 0.145 nm, Mo – 0.136 nm, Nb – 0.143 nm). The fourth group includes elements with a relatively large atomic radius (Zr – 0.160 nm, Hf – 0.159 nm), and the fifth group includes Y with a very large (0.180 nm) atomic radius. By using the elements from different groups and by modifying their concentration, it is possible to alter in a wide range the structural state and properties of high-entropy alloys [35].

Thus, for multi-element (high-entropy) materials, the accuracy of entering the required composition (up to tenths of a per cent) is a critical parameter and defines a qualitative change in the properties of materials. In this case, in order to achieve a high distortion of the crystalline lattice (which significantly decreases diffusive mobility and improves stability), the constituent elements with different parameters are used. This determines a larger selectivity of the impact of technological conditions for obtaining such materials on the formation of element composition.

Therefore, when obtaining the required properties of materials of high-entropy alloys, a very important task is to develop procedures to control the element composition. Of significant relevance for the industrial use of these materials is also the establishment of patterns in the influence of technological conditions for their obtaining on the element composition.

3. The aim and objectives of the study

The aim of present study is to identify the patterns of influence of the substrate temperature at deposition on the elemental and phase compositions of coatings obtained by electron-beam evaporation of the high-entropy alloy AlTiVCrNbMo. The identification of these patterns would make it possible to model the conditions for obtaining the required composition from the multi-element metal components with very different structure of the atom.

To accomplish the aim, the following tasks have been set:

– to compare a starting composition of the target of evaporated metal with the composition after evaporation;

– to explore peculiarities in the formation of the element composition of coatings obtained by electron-beam evaporation of the high-entropy alloy AlTiVCrNbMo at a change in the substrate temperature from 300 to 700 °C;

– to identify the features of phase formation of the coatings based on the high-entropy alloy AlTiVCrNbMo at different temperature of deposition;

– to describe the mechanism of the influence of processes at the electron-beam method of obtaining on the element composition of coatings based on high-entropy alloy AlTiVCrNbMo.

4. Procedure for obtaining ingots of high-entropy alloys and electron-beam coatings on their base

High-entropy alloys were melted in the arc furnace MIFI-9-3 in the atmosphere of high-purity argon; in this case, the atmosphere was additionally refined through repeated melting of a Zr–Ti getter. After a tenfold re-melting, high-entropy alloys were crystallized at the rate of 20 K/s in the form of a cylinder weighing 50 g. Fig. 1 shows a typical photograph of the surface of an ingot of the high-entropy alloy, which clearly demonstrates its dendrite structure.

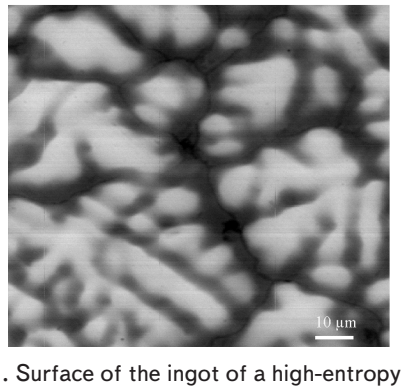

Fig. 1. Surface of the ingot of a high-entropy alloy

Vacuum condensates of the high-entropy alloy (AlTiVCrNbMo) with a thickness of 3...5 μm were obtained at the vacuum setup UVN-2M-1 at a working vacuum of $5 \cdot 10^{-5}$ mTorr [36]. Schematic of the setup for obtaining the samples is shown in Fig. 2.

The alloy evaporation was performed from water-cooled ingot mold 4 using electron-beam gun 5 with a power of 5 kW. The condensation of vapors of all the elements of the

alloy was carried out onto copper substrate 8 at temperatures 300, 500, 700 °C. Alloy condensation rate reached ~1 μm/min. Distance from the evaporators to the substrate was ~100 mm. Deposition temperature was controlled by chromel-alumel thermocouple 6.

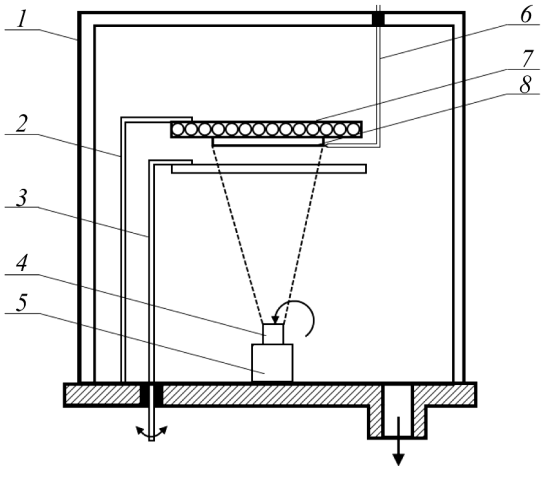

Fig. 2. Schematic of the setup for obtaining vacuum condensates: 1 — vacuum chamber; 2 — holder; 3 — shutter; 4 — water-cooling ingot mold; 5 — cathode node of electron gun; 6 — thermocouple; 7 — substrate holder; 8 — copper substrate

5. Procedures for studying the element composition and structure of the samples

Element composition of the samples was examined using the X-ray spectral method at the setup SPRUT-2 (Ukraine). The setup SPRUT-2 is a scanning crystal-diffraction spectrometer, which operates in the wavelength range from 0.035 to 7 nm (from boron to uranium) [37]. Primary excitatory radiation is the radiation from an X-ray tube of the firing type with the Ag anode at excitatory voltage 42 kV [38].

The phase-structural state was studied at the diffractometer DRON-3M (Russia) in the radiation of Cu-K_α. A graphite monochromator, installed in the secondary beam (in front of the detector), was used for monochromatizating the recorded radiation. The study of the phase composition, the structure (texture, substructure) was performed in line with traditional procedures of X-ray diffractometry by analyzing the position, intensity, and the shape of profiles of diffraction reflexes.

6. Results of studying the influence of substrate temperature during deposition on the element and phase compositions of coatings

Data on the X-ray fluorescent element analysis of the composition of an evaporated multi-element material are given in Table 1. One can see that the heaviest elements Nb and Mo with atomic masses of 92.91 and 95.96 exist in the increased content by mass, and lighter elements Al, Ti, V, and Cr (with masses of 26.98, 47.87, 50.94 and 51.99, respectively) – in mass share of about 11 %.

Table 1

Elemental composition of original evaporated material

Element	Al	Ti	V	Cr	Nb	Mo
Content, % by weight.	10.01	8.06	11.56	11.47	31.38	29.08

The scheme of the electron-beam process, employed in obtaining the coatings, leads to the formation of a coating on a large area. That is why an analysis of the element composition in two extreme points at deposition was performed in the experiment at T_s=700 °C (where the greatest non-homogeneity of the element composition on the surface area was expected). In the evaporation scheme in Fig. 3, they are shown in the form of points 1 and 2.

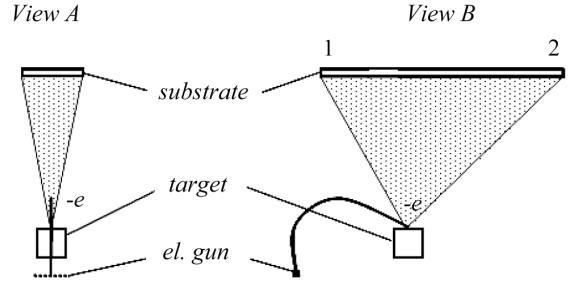

Fig. 3. Schematic of the electron-beam process of coating deposition: A — view in the plane of cross-section of electron flow from the gun on the evaporated material, B — side cross-section

We studied elemental composition using samples, located at a distance of 5 cm from the center. Typical spectra of X-ray fluorescent analysis of the element composition are shown in Fig. 4. One can see that mostly light elements (Al, Ti, Cr) and copper substrate are identified on the spectra of the coatings, obtained at the lowest T_s=300 °C. At the same time, the element composition of the coatings, obtained at a relatively high T_s=700 °C, demonstrate in the spectrum mostly the peaks, associated with heavy components (Nb and Mo), and peaks from the copper substrate.

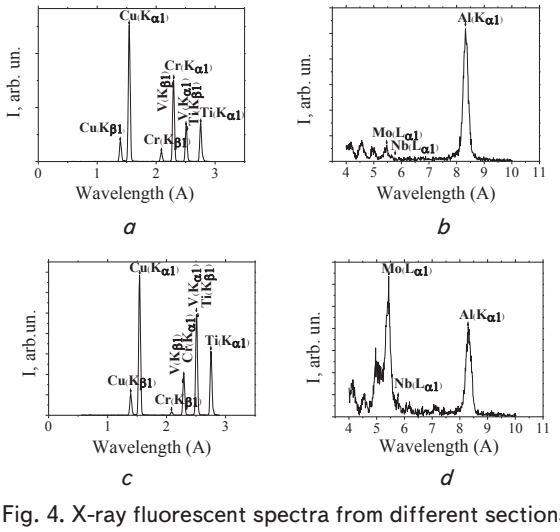

Fig. 4. X-ray fluorescent spectra from different sections of wavelengths for coatings, obtained at different temperatures: *a* and *b* — at T_s=300 °C, *c* and *d* — at T_s=700 °C

Results of the element analysis of coatings are given in the generalized form in Table 2. It follows from the obtained data that aluminum content in the coating is maximal at T_s=300 °C. At a higher temperature, aluminum content drops sharply. It should be noted that closer to the center of the substrate (position 1), a relative decrease in the aluminum content occurs to a greater extent, compared with the position that is distant from the center (position 2).

Table 2

Element composition of coatings (% by weight), obtained at different temperatures of substrate (T_s)

T_s, °C	Al	Ti	V	Cr	Nb	Mo
300	24.36	20.47	13.7	41.5	–	–
500	6.8	34.5	31.5	24.3	0.1	2.6
700 (position 1)	6.38	37.38	41.36	9	0.23	5.6
700 (position 2)	9.1	33	37.2	15.2	0.1	4.8

The chromium content in coatings changes similarly. At the same time, the content of titanium and vanadium at all temperatures of deposition remains quite high. However, the reverse process is observed for these elements at an increase in T_s (compared with aluminum and chrome). One can see that the content of Ti and V increases at an increase in T_s. At the same time, the content in coatings that are close to the center (position 1 in Fig. 3) is slightly higher than the content at the remote section 2.

The content of the heaviest and refractory niobium and molybdenum is low at all temperatures of the substrate. The content of molybdenum does not exceed 5.6 % by weight and that of niobium does not exceed 0.23 % by weight.

It is convenient to use graphical representation to visualize the shape of concentration dependences. Fig. 5 shows a graphical view of dependences of the content of elements on the substrate temperature at deposition. Fig. 5 demonstrates that all resulting dependences can be conditionally divided into 3 types (by their change). The first type includes dependences 2 and 3 (for titanium and vanadium), the course of which is characterized by a constant increase in content at an increase in T_s (type I in Fig. 5).

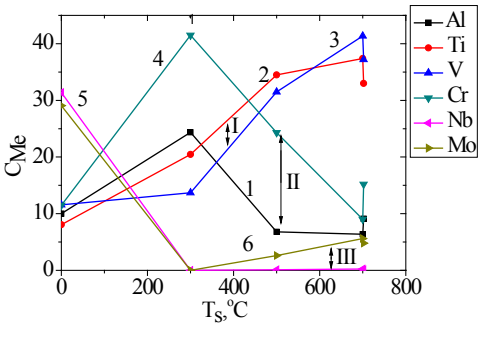

Fig. 5. Generalized dependences of element composition of coatings (C_{Me}) on the substrate temperature (T_s): 1 – Al, 2 – Ti, 3 – V, 4 – Cr, 5 – Nb, 6 – Mo. Numbers I, II, III designate characteristic types of change in the content of elements on T_s

The dependence with a maximum content at low temperature T_s=300 °C can be attributed to type II. This type of dependence is typical of aluminum and chromium (type II in Fig. 5). Changes (depending on T_s) in the content of the most refractory elements niobium and molybdenum in the coatings can be attributed to the dependence of type III (type III in Fig. 5).

The composition of the evaporated target after conducted experiments is important for the analysis of the results obtained. The obtained composition is given in Table 3. One can see that refractory Nb and Mo remained the basic elements of the target after evaporation. The content of low-melting aluminum after evaporation decreased to the greatest extent compared to the initial composition of the target (Table 1). The content of chromium in the evaporated target also decreased significantly.

Table 3

Element composition of the target after evaporation

Element	Al	Ti	V	Cr	Nb	Mo
Content, % by weight	0.33	3.7	6.82	1.48	43.7	44

The XRD-method was used in present study to determine the phase composition. Based on the data on X-ray diffraction spectra (Fig. 6), a non-homogeneous two-phase state (presumably based on BCC of lattices with periods 0.3075 nm and 0.3024 nm) is formed at a low temperature of deposition at T_s=300 °C (when there are only 4 elements in coatings). According to the element composition (Table 2), these phases can form based on chromium and a mixture of titanium and aluminum (with a large period).

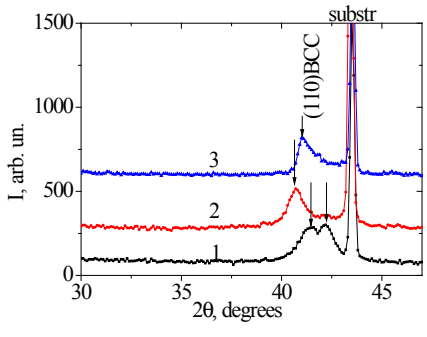

Fig. 6. Sections of X-ray diffraction spectra of coatings, obtained at different T_s: 1 – 300 °C, 2 – 500 °C, 3 – 700 °C

At high deposition temperature T_s=500 °C and T_s= =700 °C, a single-phase state is formed. This state manifests itself in the form of a single peak (shown by arrow in Fig. 6) on the diffraction spectrum of the coating obtained at T_s=500 °C. Position of the peak corresponds to the reflection from a plane (110) of BCC lattice with a period of 0.313 nm. The peak (whose position of a maximum corresponds to a period of 0.3108 nm) and an "underfur" toward large angles (Fig. 6, spectrum 3), determined by heterogeneity of element composition, appears in the spectrum at T_s=700 °C. If we compare it with the element composition, we can see that at T_s=500 °C and T_s=700 °C the number of elements in the coating is already 6. In this case, the content of five elements exceeds 2.5 % by weight.

It should be noted that the content of chromium decreases and the content of titanium and vanadium increases in the samples at an increase in the substrate temperature; Mo also appears. Since titanium has the largest atomic radius, it is possible to associate an increase in the period of a solid solution with an increase in this content.

The existence of a large asymmetry in the diffraction profile in the spectrum of the coating, obtained at the highest T_s=700 °C (spectrum 3 in Fig. 6), indicates its element heterogeneity by volume. In this case, even a small relative content of elements with large mass and reflectance (Nb and Mo), because of their great difference in atomic radius, leads to a significant increase in the spectral range and, accordingly, to the emergence of a complex profile (from several overlapping lines) of the diffraction spectrum.

7. Discussion of results of the element and phase analyses of coatings, obtained at different T_s

It follows from the results presented that the temperature of deposition plays an important role in the formation of the element and phase compositions. According to the conditions for materials formation, the results we obtained can be divided into those determined by the evaporation condition and those determined by the deposition conditions. To this end, Table 4 summarizes data on the most important characteristics of elements, which compose a high-entropy alloy (in terms of the process of electron-beam evaporation and condensation).

To analyze the influence of evaporation conditions, it is important to compare the results of research into the element composition of a target before and after evaporation. For this purpose, we will apply Tables 1, 3. The comparison shows that after evaporation the relative content of aluminum in the target decreased by 30 times (it was 10.01 and became 0.33 % by weight), of titanium – by 2.2 times (it was 8.06, and became 3.7 % by weight), of vanadium – by 1.7 times (it was 11.56 and became 6.82 % by weight), of chromium – by 7.75 times (it was 11.47 and became 1.48 %). At the same time, the relative content of niobium increased by 1.4 times (it was 31.38 and became 43.7 % by weight) and of molybdenum – by 1.5 times (it was 29.08 and became 44.0 % by weight). Thus, one can see that, by the character of evaporation, the elements that comprise a high-entropy alloy can be conditionally divided into three groups. The first group includes refractory Nb and Mo. The use of power of the electron-beam gun of 5 kW for these elements leads to the insufficient heating of the material required for their intensive evaporation. As it follows from data shown in Table 4, specific heat of vaporization of these materials is the highest and makes up 590...680 kJ/mol. The second group includes Al and Cr, which are characterized by the lowest specific heat of evaporation of 284.1...342 kJ/mol. It is possible to see that this leads to a relative decrease in the content of aluminum by 30 times, and of chromium – by 7.75 times. Ti and V, whose specific heat of evaporation is 422.6 and 460 kJ/mol, respectively, can be attributed to the third group. This led to a relative decrease in their content by 2.2 and 1.7 times, respectively.

Thus, it is clear that specific evaporation of elements from a multi-element target of high-entropy alloy proceeds in accordance with specific heat of evaporation for the constituent elements.

This parameter depends on the electron configuration of the elements (Table 4). The lowest specific heat of evaporation corresponds to one electron at the outer level of 3p or 4s shells. At the same time, the application of such parameters as melting temperature and ionization energy for analysis does not make it possible to predict all obtained experimental results by the selective evaporation of elements from multi-element materials.

Table 4

Structure and properties of coating comprising elements

Element	Atomic mass, a. e. m. (g/mol)	Electron structure	Radius of atom, pm	Melting temperature, K	Ionization energy, eV [41]	Specific heat of evaporation, kJ/mol
Al	26.9815 [39]	[Ne] $3s^2$ $3p^1$	143	933.5	18.83	284.1
Ti	47.8673[40]	[Ar] $3d^2$ $4s^2$	147	1,943	6.83-	422.6
V	50.9415[40]	[Ar] $3d^3$ $4s^2$	134	2,160	6.74	460
Cr	51.9961 [39]	[Ar] $3d^5$ $4s^1$	130	2,130	6.76	342
Nb	92.9064 [39]	[Kr] $4d^4$ $5s^1$	146	2,741	6.88	680
Mo	95.962 [39]	[Kr] $4d^5$ $5s^1$	139	2,890	7.10	590

The second factor affecting the composition is the parameters of deposition (specifically, substrate temperature at deposition). One can see from the obtained results (Table 2, Fig. 5) that the element composition at deposition also varies depending on specific heat of evaporation of condensing elements (such evaporation is called secondary in relation to the primary evaporation of a target material). If we compare results of determining the element composition, given in Tables 1, 2, we can see that compared to the target the content of aluminum at T_s=300 °C increases by 2.4 times (let us compare a decrease in the aluminum content by 30 times in the evaporated target). The content of chromium in the coating at T_s=300 °C increases larger than by 3.6 times (let us compare a decrease in the chromium content by 7.75 times in the evaporated target). Thus, even the lowest T_s=300 °C is sufficient for intensive secondary evaporation of aluminum from the growth surface. For chromium, T_s=300 °C is probably optimal for the highest growth rate. For titanium and vanadium with a higher specific heat of evaporation, compared to chrome, T_s=300 °C is even more sufficient temperature for efficient deposition. In this case, the composition is determined by the more intensive evaporation of titanium from the target (compared with vanadium).

At the highest temperature T_s=700 °C, secondary evaporation (evaporation during condensate growth on the substrate) becomes significant both for aluminum and chromium (due to low specific heat of their evaporation), which causes a substantial decrease in their content in the coating.

For Ti and V, temperature T_s=700 °C is not critical yet, which determines a continuous growth in the specific content of these elements in the coating (Fig. 5).

Against the background of decreased specific content of aluminum and chromium, the specific content of niobium and molybdenum in the coating (that is elements with the highest specific heat of evaporation) increases.

Analysis of the results of studying the phase composition reveals that in accordance with theory from [20] the existence of less than five elements in the composition (as in the case of coatings obtained at low T_s=300 °C) may fail to ensure homogeneous mixing and forming the single-phase state. A single-phase state is inherent to the coatings obtained at the higher temperature T_s=500 °C and T_s=700 °C when the coating contains at least 5 transient metal elements.

Thus, the results, obtained in present research, allow us to substantiate the principles of selection of components for forming multi-element materials of the specified composition on their basis. These results can be generalized for other methods of obtaining multi-element materials because specific heat of evaporation of the elements determines the composition depending on a general physical parameter – the temperature of heating a surface area at evaporation. In terms of the new class of materials – high-entropy alloys, this is a scientific basis for the formation of high temperature resistant, self-ordering, highly solid materials. Obtaining such materials is relevant and required by the aerospace industry, as well as general-, special-purpose, and power engineering. We plan to develop the results obtained in present work in this direction; this paper reports an analysis that was conducted for the composition of one type (AlTiVCrNbMo) only, and only one value of power (5 kW) of the electron-beam gun was applied.

8. Conclusions

1. Based on the analysis of element composition of materials for the target made of the high-entropy six-element alloy AlTiVCrNbMo before and after electron-beam evaporation, we established the critical parameter (specific heat of evaporation of the elements – a fundamental magnitude, defined by the structure of atoms of these elements), which determines the composition of the formed coating under conditions of heating at electron-beam evaporation. In accordance with specific heat of evaporation of the elements, 3 groups of elements with a characteristic change in the composition of a multi-element high-entropy alloy were distinguished.

2. It was established that at a coating deposition the element composition depends on the density of the flow of elements from the target and the processes of secondary evaporation of elements from the surface of the growing coating. The highest specific density of the flow is from the target of aluminum and chromium atoms, but even at T_s=300 °C secondary evaporation decreases specific content of aluminum in the coating.

3. It was found that for the case when a coating consists of only 4 elements (at T_s=300 °C) a single-phase coating does not form. Formation of the single-phase coating of a high-entropy alloy (based on BCC of the crystalline lattice) occurs at higher temperature T_s=500 °C when the coating contains not less than 5 elements of transient metals.

4. It was established that based on the conditions for an electron-beam process of materials formation, the obtained results can be divided into two types: those determined by the condition of evaporation of the target and those determined by the conditions of coating deposition. The density of flows of elements, evaporated from the target, is determined by their specific heat of evaporation. However, the ratio of atoms in the flow, derived in this way, may not be retained in the formed coating due to the secondary evaporation of elements from the growth surface. The results obtained allow us to substantiate the principles for selecting components in order to form on their basis the high-entropy materials with the required element and phase compositions.

References

1. Microstructural design of hard coatings / Mayrhofer P. H., Mitterer C., Hultman L., Clemens H. // Progress in Materials Science. 2006. Vol. 51, Issue 8. P. 1032–1114. doi: 10.1016/j.pmatsci.2006.02.002
2. Sobol' O. V. Structural Engineering Vacuum-plasma Coatings Interstitial Phases // Journal of Nano- and Electronic Physics. 2016. Vol. 8, Issue 2. P. 02024-1–02024-7. doi: 10.21272/jnep.8(2).02024
3. Structure of vacuum Cu–Ta condensates / Zubkov A. I., Zubarev E. N., Sobol' O. V., Hlushchenko M. A., Lutsenko E. V. // Physics of Metals and Metallography. 2017. Vol. 118, Issue 2. P. 158–163. doi: 10.1134/s0031918x17020156
4. Structural Engineering of the Vacuum Arc ZrN/CrN Multilayer Coatings / Sobol' O. V., Andreev, A. A., Gorban' V. F., Meylekhov A. A., Postelnyk H. O. // Journal of Nano- and Electronic Physics. 2016. Vol. 8, Issue 1. P. 01042-1–01042-5. doi: 10.1134/s1063784216070252
5. Structural Engineering Multiperiod Coating ZrN/MoN / Sobol' O. V., Meylekhov A. A., Stolbovoy V. A., Postelnyk A. A. // Journal of Nano- and Electronic Physics. 2016. Vol. 8, Issue 3. P. 03039-1–03039-4. doi: 10.21272/jnep.8(3).03039
6. A study of an effect of the parameters of niobium-based ion cleaning of a surface on its structure and properties / Postelnyk H., Knyazev S., Meylekhov A., Stolbovoy V., Kovteba D. // Eastern-European Journal of Enterprise Technologies. 2017. Vol. 1, Issue 5 (85). P. 34–39. doi: 10.15587/1729-4061.2017.91788
7. A Computer Simulation of Radiation-Induced Structural Changes and Properties of Multiperiod ZrNx/MoNx System / Sobol O. V., Meylekhov A. A., Bochulia T. V., Stolbovoy V. A., Gorban V. F. // Journal of Nano- and Electronic Physics. 2017. Vol. 9, Issue 2. P. 02031-1–02031-5. doi: 10.21272/jnep.9(2).02031
8. Sobol' O. V. The influence of nonstoichiometry on elastic characteristics of metastable β-WC1–x phase in ion plasma condensates // Technical Physics Letters. 2016. Vol. 42, Issue 9. P. 909–911. doi: 10.1134/s1063785016090108
9. Structural and mechanical properties of NbN and Nb-Si-N films: Experiment and molecular dynamics simulations / Pogrebnjak A. D., Bondar O. V., Abadias G., Ivashchenko V., Sobol O. V., Jurga S., Coy E. // Ceramics International. 2016. Vol. 42, Issue 10. P. 11743–11756. doi: 10.1016/j.ceramint.2016.04.095
10. Structural Engineering of the Multilayer Vacuum Arc Nitride Coatings Based on Ti, Cr, Mo and Zr / Sobol O. V., Postelnyk A. A., Meylekhov A. A., Andreev A. A., Stolbovoy V. A. // Journal of Nano- and Electronic Physics. 2017. Vol. 9, Issue 3. P. 03003-1–03003-6. doi: 10.21272/jnep.9(3).03003
11. Nanostructured coatings / A. Cavaleiro, J. T. M. De Hosson (Eds.). Springer, 2006. doi: 10.1007/0-387-48756-5
12. β-(Me_1, Me_2) and MeNx films deposited by magnetron sputtering: Novel heterostructural alloy and compound films / Musil J., Kos Š., Zenkin S., Čiperová Z., Javdošňák D., Čerstvý R. // Surface and Coatings Technology. 2018. Vol. 337. P. 75–81. doi: 10.1016/j.surfcoat.2017.12.057

13. Possibilities of structural engineering in multilayer vacuum-arc ZrN/CrN coatings by varying the nanolayer thickness and application of a bias potential / Sobol' O. V., Andreev A. A., Gorban' V. F., Stolbovoy V. A., Melekhov A. A., Postelnyk A. A. // Technical Physics. 2016. Vol. 61, Issue 7. P. 1060–1063. doi: 10.1134/s1063784216070252
14. Mixing on the Boundaries of Layers of Multilayer Nanoperiod Coatings of the TiNx/ZrNx System: Simulation and Experiment / Sobol O. V., Meylekhov A. A., Mygushchenko R. P., Postelnyk A. A., Sagaidashnikov Y. Y. // Journal of Nano- and Electronic Physics. 2017. Vol. 9, Issue 6. P. 06021-1–06021-6. doi: 10.21272/jnep.9(6).06021
15. Tuning properties and behavior of magnetron sputtered Zr-Hf-Cu metallic glasses / Zítek M., Zeman P., Zuzjaková Š., Kotrlová M., Čerstvý R. // Journal of Alloys and Compounds. 2018. Vol. 739. P. 848–855. doi: 10.1016/j.jallcom.2017.12.301
16. Miracle D. B., Senkov O. N. A critical review of high entropy alloys and related concepts // Acta Materialia. 2017. Vol. 122. P. 448–511. doi: 10.1016/j.actamat.2016.08.081
17. Raghavan R., Hari Kumar K. C., Murty B. S. Analysis of phase formation in multi-component alloys // Journal of Alloys and Compounds. 2012. Vol. 544. P. 152–158. doi: 10.1016/j.jallcom.2012.07.105
18. Structural and mechanical properties of multi-element (AlCrMoTaTiZr)Nx coatings by reactive magnetron sputtering / Cheng K.-H., Lai C.-H., Lin S.-J., Yeh J.-W. // Thin Solid Films. 2011. Vol. 519, Issue 10. P. 3185–3190. doi: 10.1016/j.tsf.2010.11.034
19. A new strategy to design eutectic high-entropy alloys using simple mixture method / Jiang H., Han K., Gao X., Lu Y., Cao Z., Gao M. C. et. al. // Materials & Design. 2018. Vol. 142. P. 101–105. doi: 10.1016/j.matdes.2018.01.025
20. Guo S., Liu C. T. Phase stability in high entropy alloys: Formation of solid-solution phase or amorphous phase // Progress in Natural Science: Materials International. 2011. Vol. 21, Issue 6. P. 433–446. doi: 10.1016/s1002-0071(12)60080-x
21. Dense and smooth amorphous films of multicomponent FeCoNiCuVZrAl high-entropy alloy deposited by direct current magnetron sputtering / Liu L., Zhu J. B., Hou C., Li J. C., Jiang Q. // Materials & Design. 2013. Vol. 46. P. 675–679. doi: 10.1016/j.matdes.2012.11.001
22. Physical metallurgy of concentrated solid solutions from low-entropy to high-entropy alloys / Cheng C.-Y., Yang Y.-C., Zhong Y.-Z., Chen Y.-Y., Hsu T., Yeh J.-W. // Current Opinion in Solid State and Materials Science. 2017. Vol. 21, Issue 6. P. 299–311. doi: 10.1016/j.cossms.2017.09.002
23. Structure and properties of two Al–Cr–Nb–Si–Ti high-entropy nitride coatings / Hsieh M.-H., Tsai M.-H., Shen W.-J., Yeh J.-W. // Surface and Coatings Technology. 2013. Vol. 221. P. 118–123. doi: 10.1016/j.surfcoat.2013.01.036
24. Microstructure and room temperature properties of a high-entropy TaNbHfZrTi alloy / Senkov O. N., Scott J. M., Senkova S. V., Miracle D. B., Woodward C. F. // Journal of Alloys and Compounds. 2011. Vol. 509, Issue 20. P. 6043–6048. doi: 10.1016/j.jallcom.2011.02.171
25. Oxidation resistance and structural evolution of (TiVCrZrHf)N coatings / Tsai D.-C., Chang Z.-C., Kuo L.-Y., Lin T.-J., Lin T.-N., Shiao M.-H., Shieu F.-S. // Thin Solid Films. 2013. Vol. 544. P. 580–587. doi: 10.1016/j.tsf.2012.12.064
26. Linder D., Holmström E., Norgren S. High entropy alloy binders in gradient sintered hardmetal // International Journal of Refractory Metals and Hard Materials. 2018. Vol. 71. P. 217–220. doi: 10.1016/j.ijrmhm.2017.11.030
27. Aging behavior of the HfNbTaTiZr high entropy alloy / Stepanov N. D., Yurchenko N. Y., Zherebtsov S. V., Tikhonovsky M. A., Salishchev G. A. // Materials Letters. 2018. Vol. 211. P. 87–90. doi: 10.1016/j.matlet.2017.09.094
28. Microstructure and properties of novel CoCrFeNiTa x eutectic high-entropy alloys / Huo W., Zhou H., Fang F., Zhou X., Xie Z., Jiang J. // Journal of Alloys and Compounds. 2018. Vol. 735. P. 897–904. doi: 10.1016/j.jallcom.2017.11.075
29. Huang P.-K., Yeh J.-W. Effects of substrate bias on structure and mechanical properties of (AlCrNbSiTiV)N coatings // Journal of Physics D: Applied Physics. 2009. Vol. 42, Issue 11. P. 115401. doi: 10.1088/0022-3727/42/11/115401
30. Structures and Characterizations of TiVCr and TiVCrZrY Films Deposited by Magnetron Sputtering under Different Bias Powers / Tsai D.-C., Shieu F.-S., Chang S.-Y., Yao H.-C., Deng M.-J. // Journal of The Electrochemical Society. 2010. Vol. 157, Issue 3. P. K52. doi: 10.1149/1.3285047
31. Dual-phase high-entropy alloys for high-temperature structural applications / Lim K. R., Lee K. S., Lee J. S., Kim J. Y., Chang H. J., Na Y. S. // Journal of Alloys and Compounds. 2017. Vol. 728. P. 1235–1238. doi: 10.1016/j.jallcom.2017.09.089
32. Wang S.-P., Xu J. (TiZrNbTa)-Mo high-entropy alloys: Dependence of microstructure and mechanical properties on Mo concentration and modeling of solid solution strengthening // Intermetallics. 2018. Vol. 95. P. 59–72. doi: 10.1016/j.intermet.2018.01.017
33. Characterization and modeling of a MoTaVWZr high entropy alloy / Anzorena M. S., Bertolo A. A., Gagetti L., Kreiner A. J., Mosca H. O., Bozzolo G., del Grosso M. F. // Materials & Design. 2016. Vol. 111. P. 382–388. doi: 10.1016/j.matdes.2016.09.006
34. Microstructure and Characterization of Mechanically Alloyed Equiatomic AlCuCrFeMnW High Entropy Alloy / Kumar D., Maulik O., Bagri A. S., Prasad Y. V. S. S., Kumar V. // Materials Today: Proceedings. 2016. Vol. 3, Issue 9. P. 2926–2933. doi: 10.1016/j.matpr.2016.09.005
35. Microstructures and transition from brittle to ductile behavior of NiFeCrMoW High Entropy Alloys / Vida Á., Chinh N. Q., Lendvai J., Heczel A., Varga L. K. // Materials Letters. 2017. Vol. 195. P. 14–17. doi: 10.1016/j.matlet.2017.02.063
36. Modifying effect of tungsten on vacuum condensates of iron / Barmin A. E., Sobol' O. V., Zubkov A. I., Mal'tseva L. A. // The Physics of Metals and Metallography. 2015. Vol. 116, Issue 7. P. 706–710. doi: 10.1134/s0031918x15070017
37. X-ray fluorescence determination of trace gold in an ion-exchange resin / Mikhailov I. F., Baturin A. A., Mikhailov A. I., Fomina L. P. // Inorganic Materials. 2014. Vol. 50, Issue 12. P. 1402–1404. doi: 10.1134/s002016851414009x
38. Mamaluy A. A., Mikhailov A. I., Fomina L. P. Optimization for the range of analytical line intensity measurement in energy-dispersion x-ray fluorescent analysis // Problems of Atomic Science and Technology. 2015. Issue 5 (99). P. 174–176.

39. Atomic weights of the elements 2011 (IUPAC Technical Report) / Wieser M. E., Holden N., Coplen T. B., Böhlke J. K., Berglund M., Brand W. A. et. al. // Pure and Applied Chemistry. 2013. Vol. 85, Issue 5. P. 1047–1078. doi: 10.1351/pac-rep-13-03-02
40. Atomic weights of the elements 2013 (IUPAC Technical Report) / Meija J., Coplen T. B., Berglund M., Brand W. A., De Bièvre P., Gröning M. et. al. // Pure and Applied Chemistry. 2016. Vol. 88, Issue 3. doi: 10.1515/pac-2015-0305
41. CRC Handbook of Chemistry and Physics / D. R. Lide (Ed.). CRC Press, 2009. 2828 p.

Запропоновано підхід до прогнозування питомого електричного опору полімерних композитних матеріалів на основі вуглецевих тканин з використанням методу скінченних елементів та аналітичних залежностей для визначення питомої електропровідності ниток. Порівняння розрахункових та експериментальних значень питомого електричного опору композитних матеріалів на основі двох типів вуглецевих тканин показали достатню достовірність запропонованого підходу

Ключові слова: композитний матеріал, вуглецеве волокно, питомий електричний опір, метод скінченних елементів

Предложен подход к прогнозированию удельного электрического сопротивления полимерных композитных материалов на основе углеродных тканей с использованием метода конечных элементов и аналитических зависимостей для определения удельной электропроводности нитей. Сравнение расчетных и экспериментальных значений удельного электрического сопротивления композитных материалов на основе двух типов углеродных тканей показали достаточную достоверность предложенного подхода

Ключевые слова: композитный материал, углеродное волокно, удельное электрическое сопротивление, метод конечных элементов

UDC 620.22-419:621.3.011.2
DOI: 10.15587/1729-4061.2018.129062

PREDICTION OF SPECIFIC ELECTRICAL RESISTIVITY OF POLYMERIC COMPOSITES BASED ON CARBON FABRICS

V. Stavychenko
PhD*
E-mail: v.stavychenko@khai.edu
S. Purhina
PhD*
E-mail: s.purhina@khai.edu
P. Shestakov*
E-mail: pashashestakov12@gmail.com
*Department of Composite Structures and Aviation Materials
National Aerospace University
named after M. Zhukovsky "Kharkiv Aviation Institute"
Chkalova str., 17, Kharkiv, Ukraine, 61070

1. Introduction

Polymeric composite materials based on carbon fabrics of different weaving have been widely used in the aerospace industry. In terms of indicators for specific strength and stiffness, carbon composites significantly outperform metals, however, they have substantially lower electrical conductivity. This must be taken into consideration when designing structural elements that may be exposed to direct and indirect effects from a lightning strike.

At present, there are many techniques to improve electrical conductivity of composite materials and structures made from them. For example, using carbon fibers with high enhanced electrical conductivity, introduction of conductive layers to composite structure, modification of a binding material employing current conductive nanoparticles, spraying of current conductive particles onto a reinforcing material or articles, etc. In addition to lightning protection systems, composites with enhanced electrical conductivity can be applied in heating elements, to shield the equipment and in other areas [1].

The application of the above methods makes it possible to create multifunctional composite materials that possess the required combination of mechanical, thermal-physical, and electrical characteristics.

Given the extending scope of application of composites in industry and increasing requirements to multifunctionality, it is a relevant task to develop reliable methods for determining their mechanical, thermal-physical, and electrical properties. At present, determining the electrical characteristics of composites is typically based on using experimental methods. These methods make it possible to obtain reliable results, but at the same time they are not effective enough when selecting the optimal structure of a composite that requires choosing from a large number of options. It is obvious that the existence of reliable calculation methods will make it possible to deal more effectively with the challenge of creating multifunctional composite materials.

2. Literature review and problem statement

The composite materials reinforced with continuous unidirectional carbon fibers have a relatively high conductivity along fibers. Specific electrical conductivity in this